


# Study on Explosion Mechanism of Dimethyl Ether/H<sub>2</sub>-Blended Gas Based on Chemical Kinetics Method

Yong Zhou <sup>1</sup>, Yang Kong <sup>2,3,\*</sup> , Qi Zhang <sup>2,3,4</sup>, Qi Huang <sup>2,3</sup>, Zhikai Wei <sup>2,3</sup> and Huaheng Lu <sup>2,3</sup><sup>1</sup> National Energy Group Wuhai Energy Co., Ltd., Wuhai 016000, China; 10790435@ceic.com<sup>2</sup> College of Safety and Environmental Engineering, Shandong University of Science and Technology, Qingdao 266590, China; zhangqi2021@sdust.edu.cn (Q.Z.); 17320500803@163.com (Q.H.); huahenglu@163.com (H.L.)<sup>3</sup> State Key Laboratory of Mining Disaster Prevention and Control Co-Founded by Shandong Province and the Ministry of Science and Technology, Shandong University of Science and Technology, Qingdao 266590, China<sup>4</sup> State Key Laboratory of Explosion Science and Technology, Beijing Institute of Technology, Beijing 100081, China

\* Correspondence: kongyang@sdust.edu.cn

**Abstract:** In order to reveal the deflagration mechanism of DME/H<sub>2</sub>-blended gasses, the micro-mechanism was studied based on the constructed UC San Diego 2016 pyrolysis oxidation mechanism model. The results show that adiabatic flame temperature and laminar flame speed increase with the increase in the equivalence ratio ( $\Phi$ ); they first increase and then decrease with the increase in the hydrogen (H<sub>2</sub>)-blended ratio ( $\lambda$ ), and with the increase in  $\lambda$ , the  $\Phi$  corresponding to the peak laminar flame speed of the blended gas increases. The addition of H<sub>2</sub> increases the consumption of O<sub>2</sub>, and H<sub>2</sub> reacts with CO to form H<sub>2</sub>O and CO<sub>2</sub>, promoting complete combustion. When  $\Phi = 1.0$ – $1.2$ , the equilibrium mole fraction of H and OH-activated radicals reach the maximum, and with the addition of H<sub>2</sub>, the concentration of activating radicals gradually increases, while the number of promoted elementary reactions increases by two, and the number of inhibited elementary reactions does not increase. Meanwhile, the addition of H<sub>2</sub> increases the reaction rate of most reactions on the main chemical reaction path CH<sub>3</sub>OCH<sub>3</sub> → CH<sub>3</sub>OCH<sub>2</sub> → CH<sub>2</sub>O → HCO → CO → CO<sub>2</sub> of DME and increases the risk of the deflagration of DME/H<sub>2</sub>-blended gas.

**Keywords:** DME/H<sub>2</sub>-blended gas; pyrolysis oxidation mechanism model; chemical reaction kinetics; equivalence ratio; hydrogen-blended ratio



**Citation:** Zhou, Y.; Kong, Y.; Zhang, Q.; Huang, Q.; Wei, Z.; Lu, H. Study on Explosion Mechanism of Dimethyl Ether/H<sub>2</sub>-Blended Gas Based on Chemical Kinetics Method. *Fire* **2024**, *7*, 328. <https://doi.org/10.3390/fire7090328>

Academic Editor: Shankar Mahalingam

Received: 1 August 2024

Revised: 27 August 2024

Accepted: 5 September 2024

Published: 20 September 2024



**Copyright:** © 2024 by the authors. Licensee MDPI, Basel, Switzerland. This article is an open access article distributed under the terms and conditions of the Creative Commons Attribution (CC BY) license (<https://creativecommons.org/licenses/by/4.0/>).

## 1. Introduction

Since the 21st century, the coordinated development of economy, energy, and environment has become the key to social sustainable development, and the development of economy, science, and technology is closely related to the degree of development and utilization of energy [1,2]. However, with the depletion of fossil fuels and the worsening of environmental pollution, countries around the world have successively put forward the concept of “carbon neutrality” and set goals in stages. For example, in September 2020, China proposed a “dual-carbon” strategic goal entitled “2030 carbon peak and 2060 carbon neutral” [3]. Due to the energy shortage and improving emission regulations, people have been conducting more and more extensive and in-depth research on fuels. Dimethyl ether (DME), as the simplest aliphatic ether, can be made from natural gas, coal, petroleum coke, or biomass as raw materials. DME is considered to be one of the cleanest fuels with the most potential for development because it does not contain a C-C bond, has high oxygen content and cetane number, good combustion performance, a short stagnation period, low NO<sub>x</sub> emissions, low combustion noise, a higher latent heat of vaporization compared to diesel fuel, and it is a kind of renewable and clean energy [4–6]. In addition, DME has high energy density, easy liquefaction, transportation, and storage, and can produce hydrogen (H<sub>2</sub>) in

the reforming reaction, so it can be used as a good safe carrier of hydrogen energy. The direct transportation of hydrogen has a very low utilization rate of hydrogen energy [7], so the Oberon Fuel Company, one of the largest fuel companies in the United States, designed and developed a hydrogenation station based on DME reforming to produce hydrogen [8].

Expanding and popularizing the scale of the hydrogen production process using DME has made it possible to use DME/H<sub>2</sub>-blended gas as a mixed fuel [9]. Meanwhile, because of the wide ignition limit and fast combustion rate of H<sub>2</sub>, adding H<sub>2</sub> to gaseous fuels can increase the combustion rate of the mixed fuel and enhance the risk of deflagration [10–12]. Therefore, the study of the micro-deflagration mechanism of DME/H<sub>2</sub>-blended gas is of great significance to its safe application.

At present, some scholars have carried out detailed studies on the deflagration characteristics of DME or H<sub>2</sub> single gas, but research on DME/H<sub>2</sub>-blended gas is still insufficient. Youn et al. [13] studied the effect of DME fuel on the performance of a four-cylinder diesel engine and found that the peak combustion pressure and ignition delay of DME fuel were higher and faster than that of ultra-low sulfur diesel, respectively. Ying et al. [14] carried out experimental studies on the combustion and emissions of a DME compression ignition engine. With the increase in the equivalence ratio ( $\Phi$ ), the peak values of pressure and temperature in the engine increased; NO<sub>x</sub> emissions decreased at first and then remained unchanged, while CO and HC emissions increased. Huang et al. [15] used high-speed ripple photography to measure the laminar flame speed of DME/air mixtures at different initial pressures and  $\Phi$ . The results showed that the Markstein number decreased with increasing  $\Phi$ . Wang et al. [16] conducted experimental and simulation studies on the propagation and extinguishing of DME/air-premixed flames and found that the high-temperature reaction of DME was mainly determined by intermediate products, and the effect of reaction kinetics on flame extinguishing was greater than that on flame propagation. Moradi et al. [17] studied the effect of H<sub>2</sub> on the combustion characteristics of a natural gas HCCI engine and found that H<sub>2</sub> improved engine efficiency, accelerated natural gas combustion, and reduced the ignition delay time and HC and CO emissions. Li et al. [18] studied the combustion characteristics of NH<sub>3</sub>/DME/H<sub>2</sub> using the spherical iso-volume combustion method and optimized the simplified kinetic mechanism, finding that H<sub>2</sub> can effectively improve the laminar combustion rate of the NH<sub>3</sub>/DME/air mixture and that the laminar flame speed shows a non-monotonous increasing trend with  $\Phi$  at different H<sub>2</sub> additions. Cong et al. [19] studied the combustion and emission characteristics of DME/H<sub>2</sub> and found that the addition of DME increased the engine power output while significantly reducing NO<sub>x</sub> emissions, but CO and HC emissions increased. Pan et al. [20] studied the variation in the ignition delay time of DME/H<sub>2</sub> mixtures with  $\Phi$  and the hydrogen-blended ratio ( $\lambda$ ) using a combination of experiments and numerical simulations and found that the ignition delay time increased with  $\Phi$  and gradually decreased and then rapidly decreased with  $\lambda$ . Shi et al. [21] analyzed a dilute DME/H<sub>2</sub> mixture with  $\Phi = 0.3\sim 0.5$  and a hydrogen mole fraction of 0~85% based on the pyrolysis oxidation mechanism model of NUI Aramco Mech 2.0 and found that when the mole fraction of H<sub>2</sub> was more than 70% and the pressure was low, while the effect of H<sub>2</sub> on the ignition delay was clearer, and there were three stages of exothermic behavior under the condition of extremely lean combustion ( $\Phi = 0.3$ ).

Up until now, scholars at home and abroad have extensively studied the chain reaction mechanism of pure DME and pure H<sub>2</sub>; however, there are relatively few studies on the pyrolysis and chemical kinetic parameters of DME/H<sub>2</sub>-blended gas in the air. It is very important to reveal the risk of deflagration of DME/H<sub>2</sub>-blended gas under different  $\Phi$  and  $\lambda$  conditions from the microscopic mechanism. In this paper, a model of the pyrolysis oxidation mechanism of DME/H<sub>2</sub>-blended gas was constructed by conducting research in the literature, and this model was validated based on the ignition delay time to determine the optimal pyrolysis oxidation mechanism model. Based on the mechanism model, adiabatic flame temperature, equilibrium molar concentration, laminar flame speed, the chemical reaction path, and related elementary reaction sensitivities were analyzed successively, and

the intrinsic effects of  $\Phi$  and  $\lambda$  on the deflagration characteristics of DME/H<sub>2</sub>-blended gas were revealed from the mechanism.

## 2. Research Methods and Pyrolysis Oxidation Mechanism Model

### 2.1. Research Methods

Based on the chemical reaction kinetic mechanism model of DME/H<sub>2</sub>-blended gas deflagration, it was assumed that 79% nitrogen and 21% oxygen would be present in the air. An equilibrium closed homogeneous 0-D reactor and premixed laminar flame-speed calculation model were adopted. The adiabatic flame temperature, laminar flame speed, equilibrium analysis, chemical reaction path, and related elementary reactions of DME/H<sub>2</sub>-blended gas with different  $\Phi$  and  $\lambda$  at the initial temperature of 298 K and initial pressure of 1 atm were analyzed. We selected  $\Phi = 0.6, 0.8, 1.0, 1.2, 1.4, 1.6, 1.8, 2.0$ ,  $\lambda = 0\%, 10\%, 30\%, 50\%, 70\%, 90\%, 100\%$ .

$\Phi$  is defined as the ratio of theoretical air consumption ( $V_0$ ) to the actual air consumption ( $V_S$ ) when burning 1 kg of fuel, i.e.,

$$\Phi = \frac{V_0}{V_S} \quad (1)$$

$$\lambda = \frac{V_{H_2}}{V_{H_2} + V_{DME}} \quad (2)$$

### 2.2. Modeling and Validation of Pyrolytic Oxidation Mechanism

In this paper, based on the UC San Diego DME model constructed by the UC San Diego 14-step DME chemical kinetic reaction model and the GRI-Mech 3.0 mechanism (containing 53 substances and 325 elementary reactions) [22], the UC San Diego 2016 model containing the H<sub>2</sub> oxidation reaction mechanism from UC San Diego is embedded [23]; thus, the DME/H<sub>2</sub>-blended gas chain reaction mechanism model was obtained. Here, the reaction mechanism model of DME/H<sub>2</sub>-blended gas is called the UC San Diego 2016 model. Through an experimental study on parameters such as the ignition delay time, explosion overpressure, and explosion temperature, many scholars at home and abroad have verified the accuracy of the UC San Diego 2016 model to predict the chemical kinetic properties of common C1-C4 substances under specific conditions. However, there are few reports on the accuracy of the UC San Diego 2016 model in predicting the chemical kinetic characteristics of DME/H<sub>2</sub>-blended gas. Therefore, it is compared with the AramcoMech 2.0 model of the National University of Galway, Ireland, which was constructed by Galway University Center for Combustion Chemistry in combination with the H<sub>2</sub> gas mixture pyrolysis oxidation mechanism of A. K eromn es, Y. Zhang, and M.  O Conaire et al [24,25].

Ignition delay time is one of the most fundamental, important, and sensitive parameters of chemical kinetics [26–29]. Pan et al. [20] revealed the ignition delay time of DME/H<sub>2</sub>-blended gas with  $\Phi = 0.5$  and an initial pressure of 1.2 atm by shock tube experiments, so the results of this experiment can be used to validate the combustion model in this paper. As shown in Figure 1, detailed comparisons of experimental and simulated values of the ignition delay time for DME/H<sub>2</sub>-doped gas under different  $\lambda$  conditions at  $\Phi = 0.5$  and an initial pressure of 1.2 atm are demonstrated so as to verify the accuracy of the UC San Diego 2016 model. Here, the blue solid line, green solid line, and red sphere represent the numerical results of the UC San Diego 2016 model, the AramcoMech2.0 model, and the experimental results of Pan et al. [20] in the State Key Laboratory of Power Engineering of Xi'an Jiaotong University, respectively.

As can be seen from Figure 1, when the UC San Diego 2016 model and AramcoMech2.0 model are used to simulate the ignition process of DME single fuel and DME/H<sub>2</sub>-blended gas, the calculation results of the AramcoMech2.0 model are slightly larger than that of the UC San Diego 2016 model, and the calculation result of the UC San Diego 2016 model is closer to the experimental results of the State Key Laboratory of Power Engineering Multiphase flow of Xi'an Jiaotong University. The UC San Diego 2016 model shows a

better ability to predict the ignition delay with higher accuracy. Therefore, in this paper, the UC San Diego 2016 model was selected as a model to study the reaction mechanism of DME/H<sub>2</sub>-blended gas.

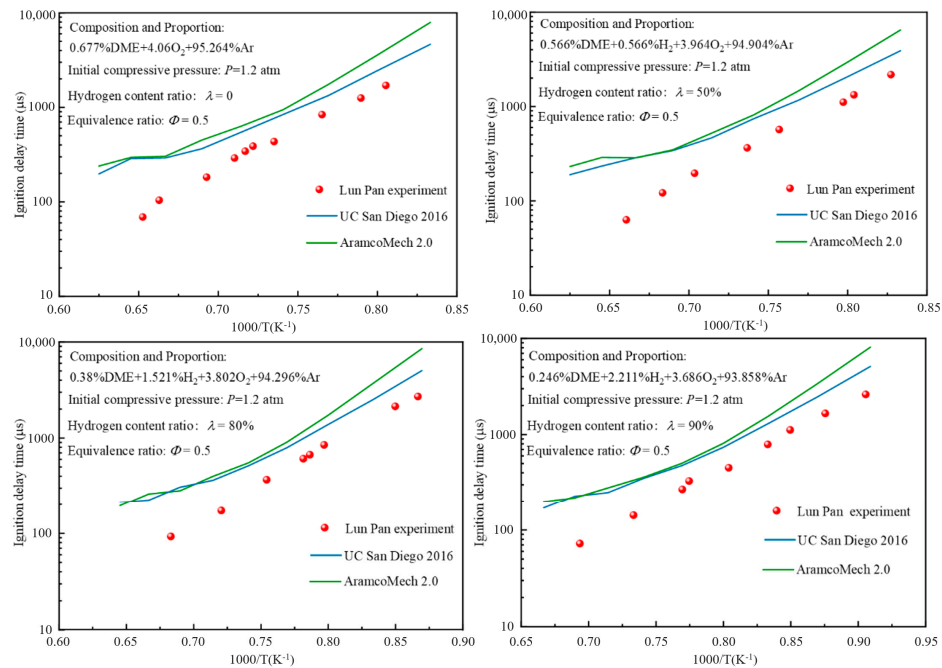


**Figure 1.** Comparison of experimental and theoretical values of ignition delay time for DME/H<sub>2</sub>-blended gas at different  $\lambda$ .

### 3. Results and Discussion

#### 3.1. Adiabatic Flame Temperature

The adiabatic flame temperature not only reflects the exothermic performance of the blended gas but also has an important influence on flame propagation and extinguishment, the ignition limit, and the formation of combustion pollutants [30,31]. Meanwhile, the adiabatic flame temperature can also reflect the laminar flame speed to a certain extent in order to help select appropriate materials and design appropriate protective measures. The adiabatic flame temperature of DME/H<sub>2</sub>-blended gas under the action of different  $\Phi$  and  $\lambda$  at normal pressure and temperature is shown in Figure 2.

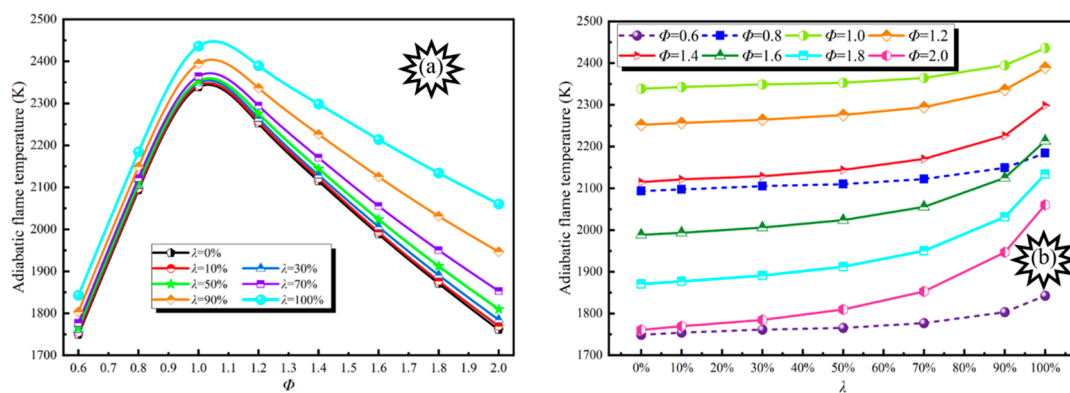


**Figure 2.** Adiabatic flame temperature evolution curves. (a). Adiabatic flame temperature evolution at different  $\lambda$ ; (b). Adiabatic flame temperature evolution at different  $\Phi$ .

From Figure 2, it can be seen that the adiabatic flame temperature first increases and then decreases with the increase in  $\Phi$  at different  $\lambda$  and reaches a maximum value between

$\Phi = 1.0$  and  $1.1$ , and the maximum value ranges from 2338 to 2436 K. At the same time, because the calorific value of DME is smaller than  $H_2$ , and there are C-O and C-C bonds in the molecular structure of  $CH_3OCH_3$  with a high bond energy, which requires larger energy to break it, the combustion reaction of  $H_2$  is relatively simple and involves only the chemical reaction of hydrogen itself. Therefore, the adiabatic flame temperature increases with the increase in  $\lambda$  under the same conditions.

The effect degree of  $H_2$  on blended gas at a lean burn concentration is much less than that of blended gas with a rich burn concentration. When  $\Phi = 0.6-2.0$ , with the increase in  $\lambda$ , the growth rate of the adiabatic flame temperature is 5.36%, 4.35%, 4.17%, 6.10%, 8.69%, 11.33%, 14.07%, and 17.01%, respectively. The growth rate of adiabatic flame temperature first decreases and then increases with the increase in  $\Phi$ , reaching a minimum value at  $\Phi = 1.0$ .

### 3.2. Laminar Flame Speed

The laminar flame speed is the velocity of a one-dimensional adiabatic plane flame surface relative to incoming unburned premixed gas. The laminar flame speed is one of the most important parameters that reflect the combustion characteristics of the fuel. The trend in laminar flame speed of DME/ $H_2$ -blended gas with  $\Phi$  and  $\lambda$  is shown in Figure 3.

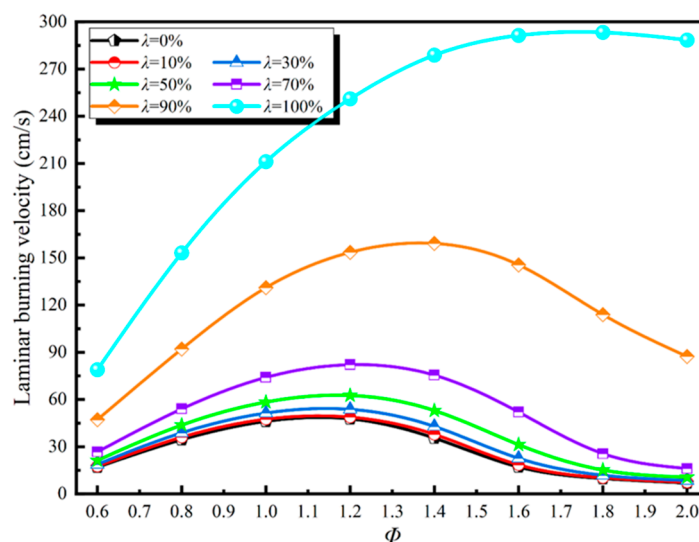


**Figure 3.** Evolution relationship between laminar flame speed,  $\Phi$ , and  $\lambda$ .

The laminar flame speed of the doped gas increases with larger  $\lambda$ , which means that increasing  $\lambda$  can increase the laminar flame speed of DME/ $H_2$ -doped gas. Meanwhile, with the increase in  $\lambda$ , the peak laminar flame speed of the blended gas corresponds to the increase in  $\Phi$ , which means that the peak laminar flame speed moves to the rich combustion condition with the addition of  $H_2$ . When  $\lambda = 100\%$ , the laminar flame speed of blended gas increases with the increase in  $\Phi$ , and when  $\lambda < 100\%$ , the laminar flame speed increases at first and then decreases with the increase in  $\Phi$ . When  $\lambda \leq 0.3$ , the laminar flame speed and evolution trend under all values of  $\lambda$  are almost the same. When the laminar flame speed increases with the increase in  $\Phi$  and the same  $\Phi$  variation, the greater the  $\lambda$ , and the greater the increase in laminar flame speed.

### 3.3. Equilibrium Molar Concentration

The risk of deflagration can be inferred by studying the equilibrium molar concentrations of reactants, which are key free radicals of the intermediate products and main products [32–34]. Figure 4 shows the equilibrium molar fraction waterfall diagram of the reactant  $O_2$  at different  $\Phi$  and  $\lambda$ .

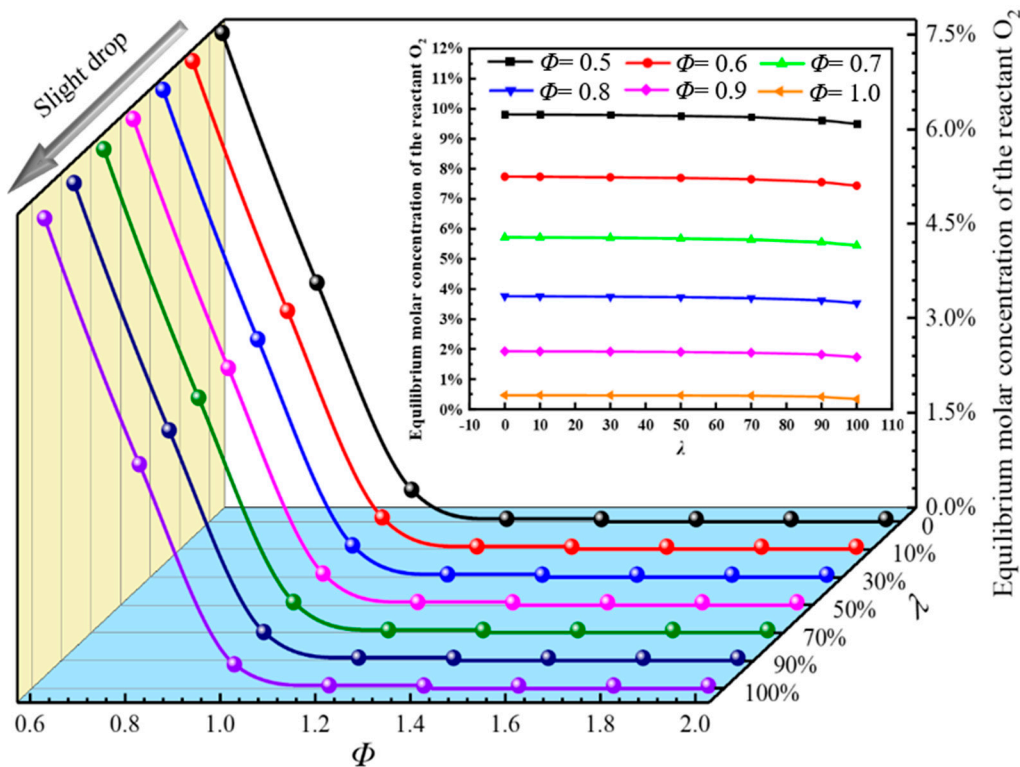


**Figure 4.** Equilibrium molar fraction of reactants of  $O_2$  for different  $\Phi$  and  $\lambda$ .

It can be seen from Figure 4 that when  $\lambda$  is the same, the equilibrium mole fraction of  $O_2$  decreases rapidly with the increase in  $\Phi$ . When  $\Phi = 1$ , there is still partial  $O_2$  in the reaction system, which is due to the reverse reaction, which leads to the re-conversion of the product into reactants, resulting in the existence of partial  $O_2$  in the reaction system after the end of the reaction. The value of  $\Phi > 1$  is present in the oxygen-lean condition, in which the sufficient blended gas results in almost the complete combustion of  $O_2$ , and the equilibrium mole fraction is close to zero.

When  $\Phi$  is the same, the equilibrium mole fraction of  $O_2$  decreases slightly with the increase in  $\lambda$ , which means that the addition of  $H_2$  increases the consumption of  $O_2$ , promotes the forward reaction of the reaction system, and increases the risk of deflagration of DME/ $H_2$ -blended gas. At the same time, when burning the same mole of gas, the oxygen consumption of  $H_2$  is much less than that of DME. Combined with Figure 2, the addition of  $H_2$  leads to a continuous increase in adiabatic flame temperature. It also shows that  $H_2$  has a “brightening effect”, which can drive the less combustible components of DME gas to burn further and consume more oxides.

H radicals can react with  $O_2$ ,  $H_2$ , and other gasses to release a large amount of heat energy. OH radicals have a stronger oxidation ability in the reaction, and they can accelerate the reaction rate through the chain reaction, thus making the reaction more intense. Figure 5 shows the equilibrium molar fraction waterfall diagram of H and OH radicals at different  $\Phi$  and  $\lambda$ .

It can be seen from Figure 5 that both H and OH radicals increase gradually with the increase in  $\lambda$ , while the OH radicals rise significantly more than H radicals with the increase in  $\Phi$ ; however, they all increase at first and then decrease with the increase in  $\Phi$ , reaching the maximum at  $\Phi = 1.2$  and  $\Phi = 1.0$ , respectively. Therefore, the overall risk of the reaction system increases with the increase in  $\lambda$ , and when  $\Phi = 1.0$ – $1.2$ , the concentration of key radicals of H and OH is the highest, and the risk is the highest. Clearly,  $H_2$  greatly increases the concentration of activated radicals in the reaction system and promotes a positive reaction.

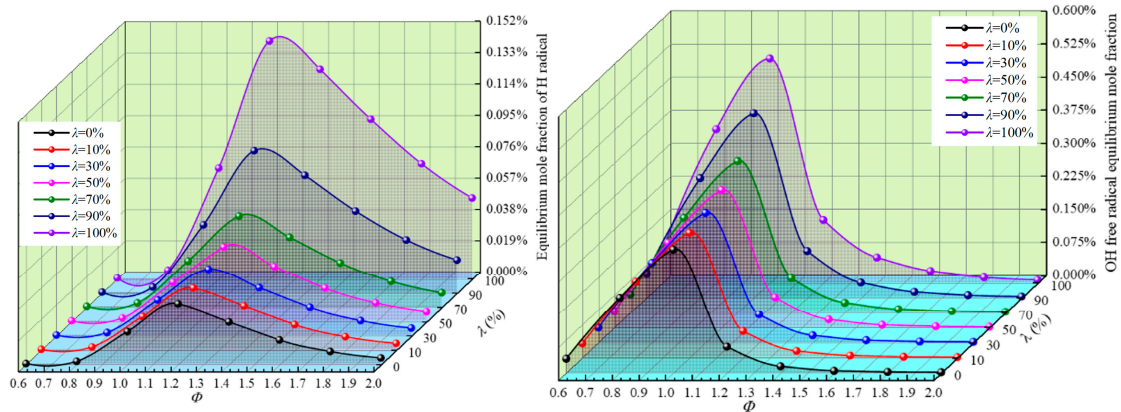
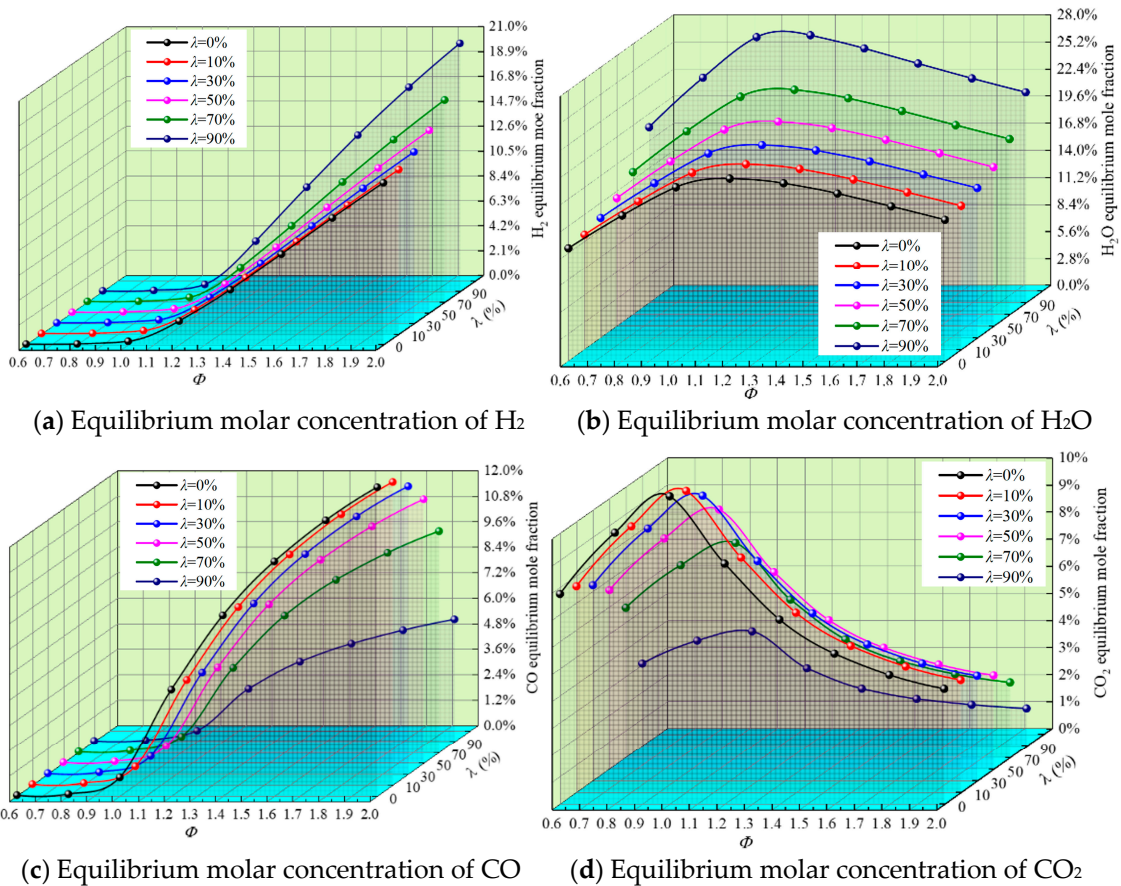


**Figure 5.** Equilibrium molar fraction waterfall diagram of H and OH radicals for different  $\Phi$  and  $\lambda$ .

In the whole reaction system, complete combustion and incomplete combustion often exist at the same time due to the change in reaction conditions and reactant characteristics. Figure 6 shows the equilibrium mole fraction waterfall diagram of the complete combustion products  $\text{CO}_2$  and  $\text{H}_2\text{O}$  and the incomplete combustion products  $\text{CO}$  and  $\text{H}_2$  under different  $\lambda$  and  $\Phi$ .



**(a)** Equilibrium molar concentration of  $\text{H}_2$

**(b)** Equilibrium molar concentration of  $\text{H}_2\text{O}$

**(c)** Equilibrium molar concentration of  $\text{CO}$

**(d)** Equilibrium molar concentration of  $\text{CO}_2$

**Figure 6.** Equilibrium molar fraction waterfall diagram of the main products for different  $\Phi$  and  $\lambda$ .

It can be seen from Figure 6 that the equilibrium concentration of  $\text{CO}_2$  and  $\text{H}_2\text{O}$  increases at first and then decreases with the increase in  $\Phi$  and peaks near  $\Phi = 1$ , when the proportion of complete reaction is the largest. With the increase in  $\Phi$ , the equilibrium concentration of  $\text{CO}$  and  $\text{H}_2$  approaches 0 at first and then increases rapidly, and incomplete combustion is especially obvious under oxygen-lean conditions.

With the increase in  $\lambda$ , the equilibrium mole fraction of  $H_2O$  increases, while the equilibrium mole fraction of  $CO_2$  decreases. It is clear that the continuous addition of  $H_2$  reduces the emissions of  $CO_2$  while promoting complete combustion. When  $\Phi > 1.0$ , the equilibrium concentration of  $CO$  decreases with the increase in  $\lambda$ . On the one hand, the increase in  $H_2$  leads to the decrease in DME supply in the reaction system, which leads to a decrease in the reaction product  $CO$ ; on the other hand, it is due to the catalytic effect of  $H_2$  on  $CO$ , so that  $H_2$  reacts with  $CO$  to produce  $H_2O$  and  $CO_2$ , releasing a large amount of heat, which results in the content of  $CO$ , which then decreases gradually.

### 3.4. Sensitivity Analysis of Elementary Reactions

In order to understand the reaction process, the temperature sensitivity of DME/ $H_2$ -blended gasses was analyzed from the point of view of the main elementary reactions [35,36]. Figure 7 shows the temperature sensitivity coefficient distribution of different  $H_2$  blending degrees ( $\lambda = 0\%, 50\%, 70\%, 100\%$ ) at  $\Phi = 1$ , including initial temperature at 298 K and initial pressure at 1 atm. Here, the positive value means promoting the reaction process, while the negative value means inhibiting the reaction process. The greater the absolute value of the sensitivity coefficient, the stronger the corresponding promotion or inhibition ability.

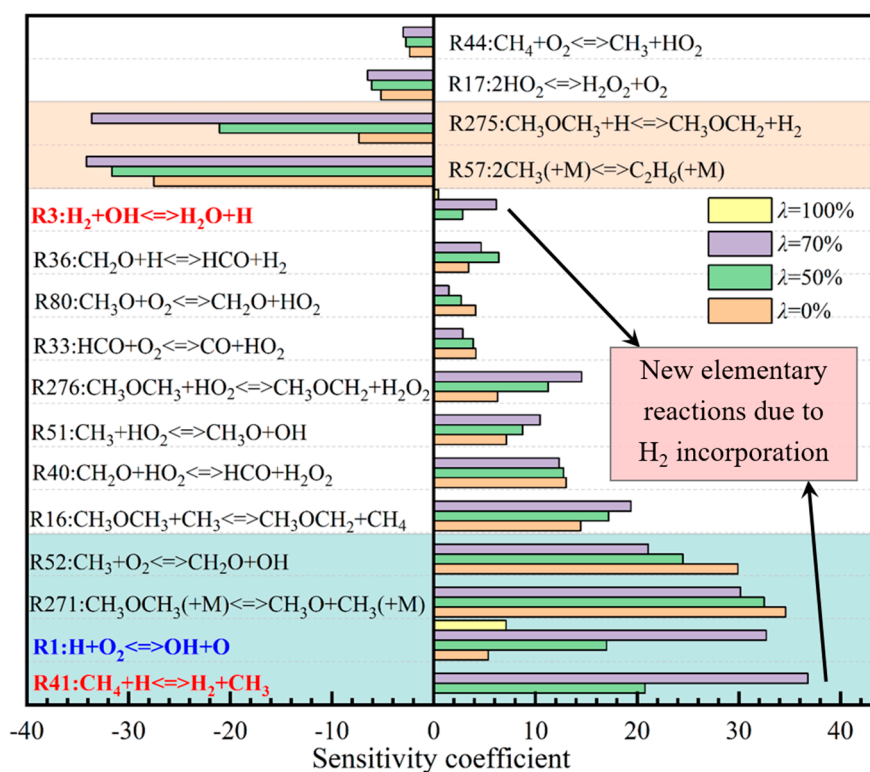


Figure 7. Sensitivity of DME/ $H_2$ -blended gas reaction system under different  $\lambda$ .

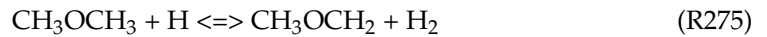
As can be seen from Figure 7, among the 16 highly sensitive radical reactions, the main reactions that promote the deflagration of DME/ $H_2$ -blended gas are as follows:



The two elementary reactions of R52 and R1 consumed  $O_2$  and produced highly active OH free radicals, which increased the concentration of active free radicals and promoted



the positive chemical reaction. Among the 16 highly sensitive radical reactions, those that had an inhibitory role on the DME/H<sub>2</sub>-blended gas reaction acted as follows:



The reaction consumes highly active H and CH<sub>3</sub> radicals, produces relatively stable ethane and H<sub>2</sub>, reduces the concentration of the activation center, and inhibits the positive process of the reaction system. At the same time, the incorporation of H<sub>2</sub> brings about two new and highly sensitive elementary reactions that promote the forward reaction process of DME/H<sub>2</sub>-blended gas, as follows:



When H<sub>2</sub> is incorporated, the number of elementary reactions that promote the positive reaction increases by two, but the number of elementary reactions that inhibit the positive reaction does not increase, and the R1, R41, R52, R275, and R276 elementary reactions are dominant. When λ = 0% and 100%, the temperature sensitivity of the R1 elementary reaction is low, but when DME and H<sub>2</sub> exist at the same time, the temperature sensitivity increases greatly, which leads to a significant increase in the active free radical OH and the reaction rate of the system. Meanwhile, it can be seen from Figure 7 that the temperature sensitivity of the promoted and inhibited elementary reactions increase with the incorporation of H<sub>2</sub>, and the absolute value of the number of promoting reactions and the absolute value of the temperature sensitivity coefficient is always larger than that of inhibitory reactions as a whole, which shows that the addition of H<sub>2</sub> can promote the chemical reaction of blended gas.

### 3.5. Chemical Reaction Path

In order to elaborate the cause and process of deflagration and to reveal the key steps in the chain reaction [37], the main pathways of the DME/H<sub>2</sub>-blended gas deflagration reaction and the main radicals, such as H, OH, O, and CH<sub>3</sub>, in each branch of the reaction were analyzed at Φ = 1.0, λ = 10%, 30%, 50%, and 70% with the initial temperature at 298 K and the initial pressure at 1 atm. The main reaction path and the radicals of the products or reactants in each branch reaction are shown in Figure 8.

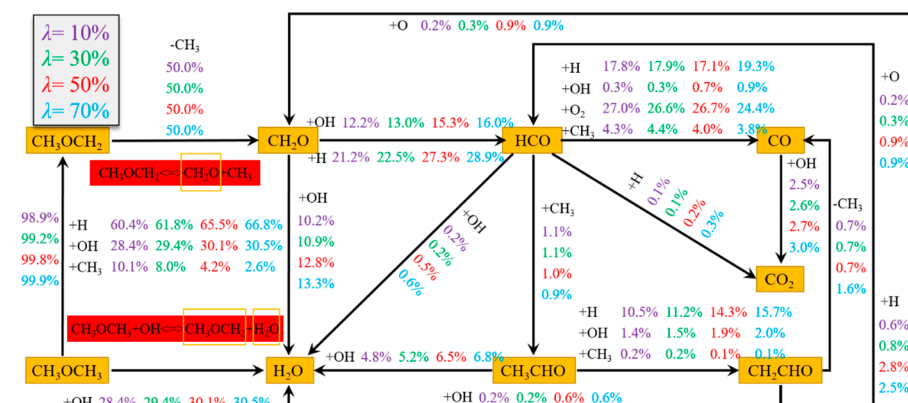


Figure 8. Schematic diagram of the DME reaction path.

From Figure 8, the main chemical reaction path of DME is CH<sub>3</sub>OCH<sub>3</sub> → CH<sub>3</sub>OCH<sub>2</sub> → CH<sub>2</sub>O → HCO → CO → CO<sub>2</sub>. For DME, about 100% of CH<sub>3</sub>OCH<sub>3</sub> undergoes dehydrogenation to form dimethyl carbonate (CH<sub>3</sub>OCH<sub>2</sub>), and H and OH are highly active radicals that play a major role in this process, in which CH<sub>3</sub>OCH<sub>3</sub> reacts with OH to form

$\text{H}_2\text{O}\cdot\text{CH}_3\text{OCH}_2$  completely through the cracking reaction to produce  $\text{CH}_3$  and the relatively stable intermediate product formaldehyde ( $\text{CH}_2\text{O}$ ).  $\text{CH}_2\text{O}$  reacts with various radicals, such as OH and H, to produce an important intermediate product aldehyde group (HCO), and most HCO is produced by reacting with H, OH,  $\text{O}_2$ , and  $\text{CH}_3$  to produce CO, which finally forms  $\text{CO}_2$  via an oxidation reaction.

With the increase in  $\lambda$ , the main reaction path of  $\text{CH}_3\text{OCH}_3$  did not change in any obvious way; only the consumption proportion of radicals changed slightly. With the increase in  $\lambda$ , the dehydrogenation of  $\text{CH}_3\text{OCH}_3$  increased from 98.9% to 99.9%, in which the H radical, which participated in the reaction, increased from 60.4% to 66.8%,  $\text{CH}_3$  continued to decrease, and the proportion of OH radicals in the main reaction pathway continued to increase. The addition of  $\text{H}_2$  increased the reaction rate of most reactions in the DME reaction process, which promoted the combustion of DME.

#### 4. Conclusions

The adiabatic flame temperature increases with the increase in  $\lambda$ ; it first increases and then decreases with an increase in  $\Phi$  and reaches the maximum value between  $\Phi = 1.0$  and 1.1, and the maximum value ranges from 2338 to 2436 K. Meanwhile, the larger the  $\lambda$ , the greater the laminar flame speed of the blended gas, and with the increase in  $\lambda$ , the  $\Phi$  corresponding to the peak laminar flame speed of the blended gas increases.

When  $\Phi = 1.0$ –1.2, the equilibrium mole fraction of H and OH-activated radicals is the highest, the activation degree of the reaction is the highest, and the risk is the greatest. The addition of  $\text{H}_2$  increases the consumption of  $\text{O}_2$  and promotes complete combustion with a decrease in CO, and  $\text{H}_2$  plays a catalytic role in CO, which makes  $\text{H}_2$  react with CO to form  $\text{H}_2\text{O}$  and  $\text{CO}_2$ , promotes the forward reaction and increases the risk of deflagration of DME/ $\text{H}_2$ -blended gas.

The elementary reactions that play a promoting role in the deflagration of DME/ $\text{H}_2$ -blended gas are mainly R1, R52, and R271, while R57 and R275 play an inhibitory role. After the addition of  $\text{H}_2$ , the number of promoted elementary reactions increases by two, while the number of inhibited elementary reactions does not increase. Meanwhile, the sensitivity coefficient of promoting and inhibiting the elementary reaction of DME/ $\text{H}_2$ -blended gas deflagration increases with the addition of  $\text{H}_2$ , which also confirms that the addition of  $\text{H}_2$  increases the risk of deflagration of blended gas from the reaction mechanism.

The main chemical reaction path of DME is  $\text{CH}_3\text{OCH}_3 \rightarrow \text{CH}_3\text{OCH}_2 \rightarrow \text{CH}_2\text{O} \rightarrow \text{HCO} \rightarrow \text{CO} \rightarrow \text{CO}_2$ . With the increase in  $\lambda$ , the main reaction path of  $\text{CH}_3\text{OCH}_3$  does not clearly change; only the consumption proportion of radicals change slightly. With the increase in  $\lambda$ , the dehydrogenation of  $\text{CH}_3\text{OCH}_3$  increases from 98.9% to 99.9%, in which the H radical, which participates in the reaction, increases from 60.4% to 66.8%,  $\text{CH}_3$  continues to decrease, and the proportion of OH radicals in the main reaction pathway continues to increase. The addition of  $\text{H}_2$  increases the reaction rate of most reactions in the DME reaction process and promotes the positive progress of DME, which promotes the positive process of DME and increases the risk of the reaction system.

**Author Contributions:** Y.Z.: Project administration, Methodology. Y.K.: Writing—Original draft, Data curation, Writing—Review and Editing. Q.Z.: Methodology, Funding acquisition. Q.H.: Investigation. Z.W.: Software, Data curation. H.L.: Data curation. All authors have read and agreed to the published version of the manuscript.

**Funding:** This work was financially supported by the Opening Project of State Key Laboratory of Explosion Science and Technology, Beijing Institute of Technology (Grant no. KFJJ23-23M).

**Institutional Review Board Statement:** Not applicable.

**Informed Consent Statement:** Not applicable.

**Data Availability Statement:** The original contributions presented in this study are included in the article, further inquiries can be directed to the corresponding author.

**Conflicts of Interest:** Author Yong Zhou was employed by the company National Energy Group Wuhai Energy Co., Ltd. The remaining authors declare that the research was conducted in the absence of any commercial or financial relationships that could be construed as a potential conflict of interest.

## References

1. Pingkuo, L.; Xue, H. ScienceDirect Comparative analysis on similarities and differences of hydrogen energy development in the World ' s top 4 largest economies: A novel framework. *Int. J. Hydrogen Energy* **2022**, *47*, 9485–9503. [[CrossRef](#)]
2. Zhang, Q.; Chen, W.; Ling, W. Policy optimization of hydrogen energy industry considering government policy preference in China. *Sustain. Prod. Consum.* **2022**, *33*, 890–902. [[CrossRef](#)]
3. Zhou, G.; Kong, Y.; Zhang, Q.; Li, R.; Qian, X.; Zhao, H.; Ding, J.; Li, Y.; Yang, S.; Liu, Y. Effect of dimensionless vent ratio on the flame-shock wave evolution dynamics of blended LPG/DME gas explosion venting. *Fuel* **2024**, *358*, 130205. [[CrossRef](#)]
4. Mogi, T.; Horiguchi, S. Explosion and detonation characteristics of dimethyl ether. *J. Hazard. Mater.* **2009**, *164*, 114–119. [[CrossRef](#)] [[PubMed](#)]
5. Bengoechea, S.; Gray, J.A.T.; Reiss, J.; Moeck, J.P.; Paschereit, O.C.; Sesterhenn, J. Detonation initiation in pipes with a single obstacle for mixtures of hydrogen and oxygen-enriched air. *Combust. Flame* **2018**, *198*, 290–304. [[CrossRef](#)]
6. Zhou, G.; Ma, Y.; Kong, Y.; Zhang, Q.; Sun, Y.; Wang, Y.; Ding, J. Study on explosion dynamics and kinetic mechanism of DME/H<sub>2</sub> blended gas at typical fuel-lean/rich concentrations. *Case Stud. Therm. Eng.* **2022**, *40*, 102444. [[CrossRef](#)]
7. Winter, C.J. Hydrogen energy—Abundant, efficient, clean: A debate over the energy-system-of-change. *Int. J. Hydrogen Energy* **2009**, *34*, 1–52. [[CrossRef](#)]
8. Zhou, G.; Ma, Y.; Kong, Y.; Zhang, Q.; Qian, X.; Liu, Z.; Wang, K.; Liu, Y.; Yang, S.; Li, Y. Influence of equivalence ratio and H<sub>2</sub> blended ratio on explosion propagation characteristics of DME/H<sub>2</sub> blended gas in closed narrow space. *Int. J. Hydrogen Energy* **2023**, *48*, 30132–30143. [[CrossRef](#)]
9. Mogi, T.; Shiina, H.; Wada, Y.; Dobashi, R. Investigation of the properties of the accidental release and explosion of liquefied dimethyl ether at a filling station. *J. Loss Prev. Process Ind.* **2013**, *26*, 32–37. [[CrossRef](#)]
10. Wei, S.; Yu, M.; Pei, B.; Ma, Z.; Li, S.; Kang, Y. Effect of hydrogen enrichment on the laminar burning characteristics of dimethyl-ether / methane fuel: Experimental and modeling study. *Fuel* **2021**, *305*, 121475. [[CrossRef](#)]
11. Rezgui, Y.; Guemini, M. ScienceDirect Effect of hydrogen addition on equimolar dimethyl ether / iso -octane / oxygen / argon premixed flames. *Int. J. Hydrogen Energy* **2017**, *42*, 29557–29573. [[CrossRef](#)]
12. Zhang, K.; Du, S.; Chen, H.; Wang, J.; Zhang, J.; Guo, Y.; Guo, J. Effect of hydrogen concentration on the vented explosion of hydrogen–air mixtures in a 5-m-long duct. *Process Saf. Environ. Prot.* **2022**, *162*, 978–986. [[CrossRef](#)]
13. Youn, I.M.; Park, S.H.; Roh, H.G.; Lee, C.S. Investigation on the fuel spray and emission reduction characteristics for dimethyl ether (DME) fueled multi-cylinder diesel engine with common-rail injection system. *Fuel Process. Technol.* **2011**, *92*, 1280–1287. [[CrossRef](#)]
14. Wang, Y.; Zhao, Y.; Xiao, F.; Li, D. Combustion and emission characteristics of a diesel engine with DME as port premixing fuel under different injection timing. *Energy Convers. Manag.* **2014**, *77*, 52–60. [[CrossRef](#)]
15. Huang, Z.; Wang, Q.; Yu, J.; Zhang, Y.; Zeng, K.; Miao, H.; Jiang, D. Measurement of laminar burning velocity of dimethyl ether–air premixed mixtures. *Fuel* **2007**, *86*, 2360–2366. [[CrossRef](#)]
16. Wang, Y.L.; Holley, A.T.; Ji, C.; Eglolfopoulos, F.N.; Tsotsis, T.T.; Curran, H.J. Propagation and extinction of premixed dimethyl-ether/air flames. *Proc. Combust. Inst.* **2009**, *32*, 1035–1042. [[CrossRef](#)]
17. Moradi, J.; Gharehghani, A.; Mirsalim, M. Numerical comparison of combustion characteristics and cost between hydrogen, oxygen and their combinations addition on natural gas fueled HCCI engine. *Energy Convers. Manag.* **2020**, *222*, 113254. [[CrossRef](#)]
18. Li, H.; Xiao, H. Effect of H<sub>2</sub> addition on laminar burning velocity of NH<sub>3</sub>/DME blends by experimental and numerical method using a reduced mechanism. *Combust. Flame* **2023**, *257*, 113000. [[CrossRef](#)]
19. Cong, X.; Ji, C.; Wang, S. Investigation into engine performance of a hydrogen-dimethyl ether spark-ignition engine under various dimethyl ether fractions. *Fuel* **2021**, *306*, 121429. [[CrossRef](#)]
20. Pan, L.; Hu, E.; Zhang, J.; Zhang, Z.; Huang, Z. Experimental and kinetic study on ignition delay times of DME/H<sub>2</sub>/O<sub>2</sub>/Ar mixtures. *Combust. Flame* **2014**, *161*, 735–747. [[CrossRef](#)]
21. Shi, Z.; Zhang, H.; Wu, H.; Xu, Y. Ignition properties of lean DME/H<sub>2</sub> mixtures at low temperatures and elevated pressures. *Fuel* **2018**, *226*, 545–554. [[CrossRef](#)]
22. Prince, J.C.; Williams, F.A. A short reaction mechanism for the combustion of dimethyl-ether. *Combust. Flame* **2015**, *162*, 3589–3595. [[CrossRef](#)]
23. Curran, H.J. Developing detailed chemical kinetic mechanisms for fuel combustion. *Proc. Combust. Inst.* **2019**, *37*, 57–81. [[CrossRef](#)]
24. Kéromnès, A.; Metcalfe, W.K.; Heufer, K.A.; Donohoe, N.; Das, A.K.; Sung, C.J.; Herzler, J.; Naumann, C.; Griebel, P.; Mathieu, O.; et al. An experimental and detailed chemical kinetic modeling study of hydrogen and syngas mixture oxidation at elevated pressures. *Combust. Flame* **2013**, *160*, 995–1011. [[CrossRef](#)]
25. Burke, U.; Metcalfe, W.K.; Burke, S.M.; Heufer, K.A.; Dagaut, P.; Curran, H.J. A detailed chemical kinetic modeling, ignition delay time and jet-stirred reactor study of methanol oxidation. *Combust. Flame* **2016**, *165*, 125–136. [[CrossRef](#)]

26. Zhang, Q.; Qian, X.; Li, R.; Zhou, G.; Sun, Y.; Ma, Y.; Kong, Y. Explosion characteristics and chemical kinetics of blended LPG/DME clean fuel based on pyrolysis and oxidation mechanism model. *Fuel* **2022**, *320*, 123896. [[CrossRef](#)]
27. Peng, C.; Zou, C.; Ren, J.; Lin, Q.; Xia, W.; Luo, J.; Xiao, Y. Ignition delay times of C<sub>2</sub>H<sub>4</sub>, C<sub>2</sub>H<sub>4</sub>/n-C<sub>4</sub>H<sub>10</sub>, and n-C<sub>4</sub>H<sub>10</sub>/i-C<sub>4</sub>H<sub>10</sub> under O<sub>2</sub>/CO<sub>2</sub> atmospheres: Shock tube experiments and kinetic model. *Combust. Flame* **2023**, *254*, 112825. [[CrossRef](#)]
28. Burnett, M.A.; Daniels, C.; Wei, L.; Wooldridge, M.S.; Wang, Z. A computational and experimental study of the effects of thermal boundary layers and negative coefficient chemistry on propane ignition delay times. *Combust. Flame* **2023**, *257*, 112415. [[CrossRef](#)]
29. Huang, Y.; Jiang, C.; Wan, K.; Gao, Z.; Vervisch, L.; Domingo, P.; He, Y.; Wang, Z.; Lee, C.H.; Cai, Q.; et al. Prediction of ignition delay times of Jet A-1/hydrogen fuel mixture using machine learning. *Aerosp. Sci. Technol.* **2022**, *127*, 107675. [[CrossRef](#)]
30. Aliyu, M.; Abdelhafez, A.; Nemitallah, M.A.; Said, S.A.M.; Habib, M.A. Effects of adiabatic flame temperature on flames' characteristics in a gas-turbine combustor. *Energy* **2022**, *243*, 123077. [[CrossRef](#)]
31. He, X.; Liu, Z.; Jiang, H.; Yang, Q.; Jiang, Z.; Feng, G.; Zhao, C. Super adiabatic flame temperature phenomenon for NH<sub>3</sub>/O<sub>2</sub>/N<sub>2</sub> mixtures. *Fuel* **2023**, *346*, 128264. [[CrossRef](#)]
32. Clará, R.A.; Marigliano, A.C.G.; Campos, V.d.V.; Sólamo, H.N. Density, viscosity, vapour-liquid equilibrium, excess molar enthalpy, and their correlations of the binary system [1-pentanol + R-(+)-limonene] over the complete concentration range, at different temperatures. *Fluid Phase Equilib.* **2010**, *293*, 151–156. [[CrossRef](#)]
33. Yang, Q.C.; Qiu, D.F.; Dang, Y.L.; Qiao, Z.P.; Xu, Z. Phase equilibrium systems of CsX + MnX<sub>2</sub> + H<sub>2</sub>O (X = Cl, Br) at 298.15 K and standard molar enthalpy of formation of CsMnX<sub>3</sub>·2H<sub>2</sub>O and Cs<sub>2</sub>MnX<sub>4</sub>·2H<sub>2</sub>O. *J. Chem. Thermodyn.* **2021**, *161*, 106541. [[CrossRef](#)]
34. Mu, X.; Cong, H.; Shao, Z.; Yuan, Z.; Zhu, B.; Zhang, K.; Bi, M.; Wang, X. Experimental and theoretical research on the inhibition performance of ethanol gasoline/air explosion by C<sub>6</sub>F<sub>12</sub>O. *J. Loss Prev. Process Ind.* **2023**, *83*, 105088. [[CrossRef](#)]
35. Yu, M.; Li, S.; Li, H.; Han, S.; Wang, F.; Lou, R.; Zheng, K.; Yu, Y. Numerical evaluation of the influence of initial pressure/temperature on the explosion properties and soot formation of methane/coal volatiles mixtures. *Fuel* **2023**, *331*, 125698. [[CrossRef](#)]
36. Zhao, Z.; Liang, Y.; Guo, B.; Song, S.; Bai, J. Explosion dynamics of premixed LPG/H<sub>2</sub> fuel in a confined space. *Int. J. Hydrogen Energy* **2023**, *48*, 36211–36221. [[CrossRef](#)]
37. Shang, S.; Bi, M.; Gao, W. Investigation on synergistic suppression of hydrogen explosion behaviors by ethylene and carbon dioxide. *J. Loss Prev. Process Ind.* **2024**, *87*, 105214. [[CrossRef](#)]

**Disclaimer/Publisher's Note:** The statements, opinions and data contained in all publications are solely those of the individual author(s) and contributor(s) and not of MDPI and/or the editor(s). MDPI and/or the editor(s) disclaim responsibility for any injury to people or property resulting from any ideas, methods, instructions or products referred to in the content.